Research Article | Vol. 28, No. 9 / 27 April 2020 / Optics Express 12675
Optics EXPRESS

Radiation pressure-induced nonlinearity in a micro-droplet

ARAM LEE,[1,2] PENG ZHANG,[3] YONG XU,[1,5] AND SUNGHWAN JUNG[4,6]

[1]Department of Electrical and Computer Engineering, Virginia Tech, Blacksburg, VA 24061, USA
[2]Institute of Advanced Composite Materials, Korea Institute of Science and Technology (KIST), 92 Chudong-ro, Bongdong-eup, Wanju-gun, Jeonbuk 55324, South Korea
[3]Department of Mechanical and Aerospace Engineering, New York University Tandon School of Engineering, Six MetroTech Center, Brooklyn, New York 11201, USA
[4]Department of Biological and Environmental Engineering, Cornell University, Ithaca, NY 14853, USA
[5]yong@vt.edu
[6]sunnyjsh@cornell.edu

Abstract: In recent years, some of the most interesting discoveries in science and engineering emerged from interdisciplinary areas that defy the traditional classification. One recent and extensively studied example is the advent of optomechanics that explores the radiation pressure-induced nonlinearity in a solid micro-resonator. Instead of using a solid resonator, we studied a liquid droplet resonator in which optical pressure could actively interact with the fluid interface. The droplet resonator supported high-quality whispering gallery modes along its equatorial plane, which produced a radiation pressure that counterbalances the interfacial tension, resulting in a droplet with damped harmonic oscillation. A major goal of this study was to demonstrate that such a novel and all-liquid platform could lead to a single-photon-level nonlinearity at room temperature. If successful, such a highly nonlinear system may lead to new research paradigms in photonics, fluid mechanics, as well as quantum information science.

1. Introduction

Photon-phonon coupling in high quality (Q) optical resonators have been studied to understand many interesting physical phenomena such as the mechanical oscillations driven by the back-action of photons in optical cavities [1–4]. To date, research on optomechanics primarily focused on the photon resonance in solid cavities itself [5–8], or by submerging them in liquid cladding medium [9–12], more intriguing scenario of fluid-mechanical interaction of solid core and liquid cladding became available. However, to achieve optomechanical interactions at ultralow optical power, i.e., few-photon regime, choosing liquid as core material of optical resonator as well should be more natural due to its overwhelming deformability over the solid micro-structures under external stimuli. In fact, a pioneering study on the interplay between the radiation pressure and a liquid [13] was carried out decades ago, which observed an intriguing phenomenon of an air-water interface deformation induced by an intense laser beam. Although there have been follow-up studies on the optofluidic interaction by means of direct excitation of laser onto the flat liquid interfaces [14–17] or droplet surfaces [18–20], in the absence of either an effective optical power coupling to the interface or the resonant power amplification, these novel findings have not led to practical applications that are operational at low optical power.

Fortunately, through a unique optical mode coupling into a spherical cavity using a tapered fiber, recent studies on whispering gallery modes (WGMs) have facilitated the efficient coupling of optical power into a droplet [21–25], which also provides high power amplification by serving itself as a whispering gallery resonator (WGR). These advancements in experimental techniques have enabled the observation of kilohertz droplet capillary resonances [26,27] and megahertz

#386777 https://doi.org/10.1364/OE.386777
Journal © 2020 Received 14 Jan 2020; revised 7 Apr 2020; accepted 7 Apr 2020; published 14 Apr 2020

Optics EXPRESS

acoustic resonances [28,29], where both were enhanced by the optofluidic interactions inside the droplet WGMs.

In this paper, we showed an experimental verification of our previous theoretical prediction of measurable resonance shift by WGM-induced radiation pressure in a liquid resonator [30]. Unlike other reports regarding the optically excited free-vibrational motion in a droplet, i.e., capillary/acoustic resonances described above, we focused more on the highly damped response by introducing a viscous microdroplet. Such an overdamped system offered us an access to the steady-state response of the droplet, in which the steadily excited WGM (outward radiation pressure) and surface tension (inward recovery force) balances each other. The formation of radiation pressure along the equatorial circumference of a droplet resulted in a bulged deformation of a sphere to an oblate spheroid, which provided us a direct measure of radiation pressure by shifting the WGM resonance.

In addition to the radiation pressure, we have also theoretically analyzed a wide range of optofluidic nonlinearities in a droplet associated with the Kerr effect, thermal expansion, thermo-optic effect, thermocapillary, and light scattering-induced optical force [31,32]. Through our comparative analysis, the radiation pressure was found to have a dominating effect on the optical nonlinearity of the liquid resonator. Here, toward a realistic verification of our theoretical predictions, we designed a series of experiment to quantify the dynamic optical behavior of a liquid resonator coupled with a WGM. Specifically, we scanned the laser wavelength across the WGM resonance wavelength with different speeds and directions. We recorded such optofluidic interplay in time domain and demonstrated that the WGM-induced nonlinearity is dominantly produced by the radiation pressure. Moreover, it is confirmed that the observed temporal response agrees well with our harmonic oscillator (HO) model derived from the analytical solution of the radiation pressure in [30], where the fluid-mechanical parameters of model followed the definitions given by [19,33,34]. Such a strong nonlinearity of radiation pressure led us to an alluring conclusion that in a liquid droplet with an ultralow but experimentally attainable interfacial tension, the presence of a WGM by even a single photon could produce a measurable shift in its resonance wavelength, and experimental realizations of room temperature single-photon-level nonlinearity are also feasible.

2. Experimental framework: characterization of a liquid droplet WGR

To measure the shift of WGM resonance under different input optical powers (P_{in}) injected through a single-mode taper, we adopted a standard experimental configuration of taper-droplet resonator coupling and the transmission measurement as shown in Fig. 1(a). The taper was placed at a proximate to the equator of droplet resonator and the taper-resonator coupling distance was tuned by a piezo-stage (P611.3s, Physik Instrumente) with its positioning resolution of 1 nm, while two CCD cameras monitored the relative position from side and top. The optical transmission was firstly excited by a CW tunable laser (TLB-6711, New Focus, 729-739 nm) and measured by a 10 MHz photodetector with adjustable gain (2117-FC, New Focus).

The high-Q resonator (core) was a drop of index matching fluid (IMF, Perfluorocarbon and Chlorofluorocarbon, AAA13600, Cargille) with its radius $R \approx 250\ \mu m$, whose optomechanical properties are accurately manufacturer-calibrated, and it was mounted on a stem which was built in a water chamber (cladding) as shown in Fig. 1(b). A cross-sectional illustration of the fundamental WGM confined in the equatorial plane of the droplet resonator is shown on the right as well. Other optofluidic parameters of the core and cladding liquids are listed in Table 1.

By scanning an output wavelength of a tunable laser (λ) at around 780 nm, we could measure the transmission coefficient T (ratio of output to input power) of the taper-droplet system as a function of λ. Figure 1(c) shows a typical transmission spectrum of the droplet resonator, which contains multiple sharp dips, each associated with a high-Q WGM. Experimentally, the free-spectral-range (FSR) of the droplet was found to be 258 pm, which closely matches the

Optics EXPRESS

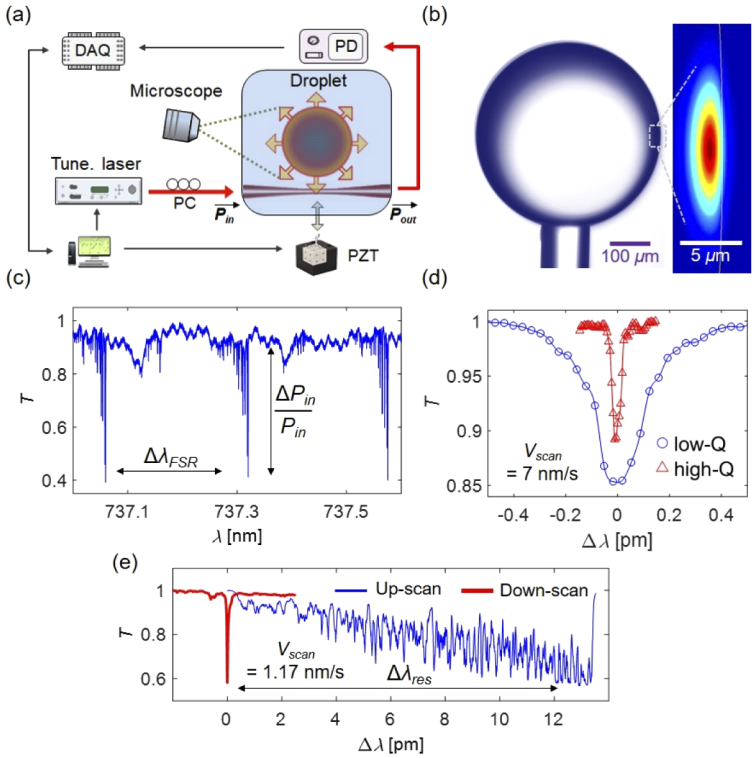

Fig. 1. Experimental configuration and characterization of a droplet WGR. (a) Schematic diagram of the droplet WGM experimental setup (DAQ: data acquisition, PD: photodetector, PC: polarization controller, PZT: piezoelectric transducer). (b) Illustration of a droplet resonator (left) and the WGM pattern in r-θ plane (right). (c) WGM transmission spectrum of a droplet resonator. (d) Examples of high-Q droplet resonances (blue: $Q = 2.1 \times 10^6$, red: $Q = 1.7 \times 10^7$) ($\Delta P_{in} = 8$ μW). (e) Typical nonlinearities in WGM resonances observed during up-scan (blue) and down-scan (red) ($\Delta P_{in} = 200$ μW).

Table 1. Optofluidic parameters of core and cladding of liquid WGR configuration[a]

	α (1/m)	n (RIU)	σ (mN/m)	μ (mPa·s)	ρ (kg/m^3)
Core (IMF)	0.26	1.357	18	16	1917
Cladding (water)	2	1.330	72	1	1000

[a]α: absorption coefficient, n: refrative indx, σ: surface tension, μ: viscosity, ρ : density

estimate given by $\Delta\lambda_{FSR} = \lambda^2/(2\pi nR) = 253$ pm. For any given resonance dip, we used ΔP_{in} to denote the difference in transmitted optical power between the on- and off-resonance cases, as indicated by a vertical arrow in Fig. 1(c).

In the estimation of optical loss in our droplet resonator, given the relatively large size of our droplet compared to the visible wavelength (> a few hundred folds), we estimated that its radiative loss is very low so as the radiation limited Q-factor becomes very high ($Q_{\text{rad}} = 7 \times 10^8$) [35]. Also, we varied the coupling coefficient (κ) between the taper and the droplet resonator by manipulating the gap distance between them, which allowed us to tune the values of ΔP_{in} and on-resonance transmission coefficent ($T_{on} = 1 - \Delta P_{in}/P_{in}$). To minimize the taper-resonator coupling loss, we operated in the under-coupled regime with T_{on} varying in a range of 0.2 to 0.7 [36]. Therefore, the total intrinsic Q-factor can be simply denoted by the inverse sum of the

Optics EXPRESS

remaining two different Q-factors limited by scattering at droplet surface (Q_{scat}) and material absorption in the volume (Q_{abs}).

Due to the thermodynamic motion of resonator fluid at room temperature, the quality of core-cladding interface may experience random thermal fluctuation, but considering the surface tension of droplet fluid (σ = 18 mN/m), the RMS scale of such perterbation is expected to be as small as molecular level. Refering to the theoretical analysis of potential quality factor of droplet resonator [37], the scattering limited Q-factor is found to be as high as $Q_{scat} = 50\sqrt{\sigma R^2/k_B T_K} = 2.6 \times 10^7$ (k_B: Boltzmann constant, T_K: absolute temperature). In addition, using the attenuation coefficient (α) of the droplet fluid at the wavelength of our interest (780 nm) which is given by the manufacturer, the absorption-limited Q-factor was found to be $Q_{abs} = 2\pi n/\alpha\lambda = 3.5 \times 10^7$, which finally resulting in the upper limit of intrinsic quality of our droplet resonator as $Q = 1/(1/Q_{scat} + 1/Q_{abs}) \sim 1.5 \times 10^7$.

To experimentally confirm the above-discussed intrinsic Q-factor, we first estimated the full width at half maximum (FWHM) of a resonance, which was excited with very low input power (8 μW) at a fast wavelength scan speed (V_{scan} = 7 nm/s) to avoid any forms of nonlinearities that may distort the spectral shape of the resonance, and found that the Q-factor ($Q = \lambda_{res}/FWHM$) typically varied in a range of 10^6 to 10^7. Due to the Q-factor highly related to the absorption mechanism in our droplet WGM, variations in its value could potentially be attributed to the presence of contaminants in the core and cladding liquids. Figure 1(d) shows two representative examples of the droplet resonance spectra measured at low input powers (cold resonances) (blue: lower $Q \sim 2.1 \times 10^6$, red: higher $Q \sim 1.7 \times 10^7$), and notably, the higher Q is reasonably close to the aforementioned theoretical upper limit.

Next, to experimentally characterize the radiation pressure-induced nonlinearity, we scanned the transmission spectrum of the coupled taper-droplet system at reasonably slow wavelength scan speed (V_{scan} = 1.17 nm/s) and relatively high input power (ΔP_{in} = 200 μW), and the results are shown in Fig. 1(e). Interestingly, we found that the shape of WGM transmission completely changed depending on the direction of laser scan. Here, we used a term 'up-scan' (or 'down-scan') to denote a case where we increased (or decreased) the tunable laser wavelength. For up-scan, we found that the WGM transmission (blue curve in Fig. 1(e)) had a gentle downward slope followed by a sharp recovery that was often reported in the previous studies of WGM-induced nonlinearities [25,38,39]. We used $\Delta\lambda_{res}$ to represent the magnitude of red-shift during up-scan which is indicated by a horizontal arrow in Fig. 1(e).

In contrast, as it can be seen as red curve in Fig. 1(e), the resonance spectrum observed in down-scan tends to exhibit extremely narrow FWHM, which is even thinner than the one found in cold resonance. Qualitatively, the red-shift of WGM resonance observed during up-scan can be explained as follows. As the tunable laser wavelength approached a WGM resonance from the blue-side, the optical power carried by the WGM increased and the following enhanced radiation pressure could deform the droplet and push its interface outwards, leading to a red-shift of the resonance. With a reasonably slow scan speed, the tunable laser wavelength potentially matched the resonance shift and produced the transmission spectrum in Fig. 1(e) (blue curve). The noise in down-slope was attributed to the noise in the input laser wavelength/power [39] and thermally driven fluctuation of droplet interface [27,37]. For down-scans, the directions of laser scan and the radiation pressure-induced resonance shift were opposite, which therefore produced narrower resonance FWHM as shown in Fig. 1(e) (red curve). More details on the variations of resonance shapes in up/down scans are further discussed in next chapters.

Similar pattern of resonance shift has also been demonstrated in the study of nonlinearity in solid resonators [38,39], where the shifts were accounted for the positive thermo-optic coefficient and thermal expansion by optical heating. However, in our case, the use of liquid resonator with negative thermo-optic coefficient blue-shifts the resonance and counteracts the red-shift by thermal expansion. Our previous theoretical estimations of these two nonlinearities in liquid

Optics EXPRESS

resonator [31,32] revealed that the two factors nearly cancel each other out, and in addition, other's experiment conducted with water drop [25] even reported a thermally blue-shifted WGM resonance, where thermo-optic effect dominated thermal expansion.

For a comparative analysis, we estimated the scale of thermal nonlinearities by equating the coupled optical power during the up-scan in Fig. 1(e) to the generated thermal energy ($E_{therm} = \int(P_{in} - P_{out})dt = 4.8 \times 10^{-7} J$). Assuming the resulted heat is evenly distributed in the resonator volume, the temperature change can be calculated as $\Delta T_T = E_{therm}/C_p VD = +0.002°\mathrm{C}$ from the given density ($D = 1917\ kg/m^3$), specific heat ($C_p \sim 2000\ J/kg/°\mathrm{C}$), and radius ($R_0 = 250\ \mu m$) of the droplet resonator. Introducing the thermo-optic coefficient ($dn/dT_T = -0.00034°\mathrm{C}^{-1}$) and thermal expansion coefficient ($\alpha_T = +0.001\ cc/cc/°\mathrm{C}$) of index matching fluid, the thermally induced WGM resonance shift is found to be approximately $\Delta\lambda_{res,\,therm} = \lambda\left(\frac{1}{n}\frac{dn}{dT_T} + \frac{1}{3}\alpha_T\right)\Delta T_T = 780\ \mathrm{nm}(1.5 \times 10^{-7}) = +0.12\ \mathrm{pm}$, which is negligible compared to the shift observed in Fig. 1(e). Based on above analogy, we hereby claim that all of experimental result in our current study is red-shifted WGM resonance in liquid resonator, which were mainly induced by the outward radiation pressure due to circulating optical power of WGM.

3. Theoretical framework: the harmonic oscillator model

The dynamical coupling between the optical field and a liquid droplet could be modeled as a harmonic oscillator. Specifically, we phenomenologically described the radiation pressure induced droplet deformation as:

$$\Delta\ddot{R} + 2\mu_L\Delta\dot{R} + \omega_L^2\Delta R = \omega_L^2 R_0\frac{P_{WGM}}{P_{sat}}, \tag{1}$$

where the overdots indicate time derivatives, ΔR is the time-dependent changes in droplet radius at the equator (i.e., $\theta = \pi/2$), P_{WGM} is the total power of the WGM, and P_{sat} is a constant representing a saturation power [30]. The damping constant ($\mu_L = (2L+1)(L-1)\mu/(\rho R_0^2)$) and the oscillation frequency ($\omega_L^2 = L(L+2)(L-1)\sigma/(\rho R_0^2)$) are respectively given by [19,33,34], where we consider only the fundamental mode ($L = 2$). In deriving Eq. (1), we assumed that the polar dependence of the change in droplet radius could be described by the lowest spherical harmonic function ($Y_{L=2,M=0} = \sqrt{5/16\pi}(3cos^2\theta - 1)$) [30], which is a reasonable approximation confirmed by the comparison with an exact solution as shown in Fig. 2(a). The right hand side of Eq. (1) is associated with the radiation pressure, which is propotional to the WGM power (P_{WGM}). At steady state, Eq. (1) is reduced to $\Delta R/R_0 = P_{WGM}/P_{sat}$. The relative change in droplet radius ($\Delta R/R_0$) can be determined from the proportionality constant (P_{sat}) at a given P_{WGM}, which can be estimated (in a closed form expression as well) by the method given in [30]. Assuming the P_{WGM} as unity (= 1 W), the values of $\Delta R/R_0$ determined by the fluidic parameters of our droplet ($\sigma = 18$ mN/m) at various radii are shown as red curve in Fig. 2(b). Two more results at ultralow interfacial tensions are also shown (green: $\sigma = 10^{-1}$mN/m, blue: 10^{-3} mN/m), suggesting that $\Delta R/R_0$ is proportional to $1/\sigma R_0$.

A change in the droplet radius was expected to be accompanied by a shift in its WGM resonance. A WGM phase shift ($\phi(t)$) and the magnitude of the droplet deformation at the equator ($\Delta R(t)$) satisfy $\phi(t) = \phi_0 + 4\pi^2 n_{eff}(R_0 + \Delta R(t))/\lambda(t)$, where n_{eff} is the effective index of the WGM, which can be well approximated to be n_{core} due to the strongly confined WGM inside the droplet surface. In our experiment, the laser wavelength ($\lambda(t)$) is scanned at a speed V_{scan} and can be described as $\lambda(t) = \lambda_0 + V_{scan}t$. Following the analysis in [40], we can express P_{WGM} and the transmitted power (P_{trans}) as a function of the input power (P_{in}) as

$$P_{WGM} = \frac{\tau_r^2\kappa^2}{|\tau_r\tau_c - \exp(-i\phi(t))|^2}P_{in}, \tag{2.1}$$

Optics EXPRESS

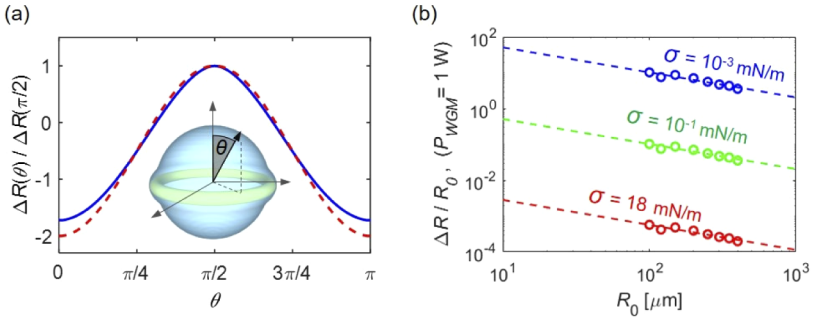

Fig. 2. Theoretical analysis of droplet deformation. (a) Polar dependence of droplet deformation (blue solid curve: exact solution, red dashed curve: lowest spherical harmonic expansion ($L = 2$)). (b) Radiation pressure induced droplet deformation ($\Delta R/R_0$) for our droplet samples with different radii (red) at $P_{WGM} = 1$ W. Two other results are estimated using the same liquid properties but ultralow interfacial tensions.

$$P_{trans} = \frac{|\tau_r - \tau_c \exp(-i\phi(t))|^2}{|\tau_r \tau_c - \exp(-i\phi(t))|^2} P_{in}, \tag{2.2}$$

where τ_c and $\kappa = \sqrt{1-\tau_c^2}$ are, respectively, the throughput and cross-over coupling between the taper and the droplet, and τ_r accounts for the round trip attenuation of the WGM. It should be noted that these three WGM parameters (τ_c, τ_r, and κ) are assumed to be independent of P_{in} because, though the droplet deformation changes the taper-resonator gap distance as well as the coupling condition, the scale of deformation in our study at P_{in}<200 μW is expected to be as small as a few nanometers, incurring little effect on the state of the under-coupled WGM. Equations (1), (2.1), and (2.2) together describe the nonlinear coupling between the optical field and the liquid droplet, whereby the WGM deforms the droplet through radiation pressure, and the deformed droplet in turn shifts the resonance of the WGM by changing $\phi(t)$.

4. Results

4.1. Resonance spectra during up-scan

To experimentally investigate the relationship between $\Delta\lambda_{res}$ and ΔP_{in}, we measured about 6000 different transmission spectra (> 1000 for each V_{scan}) for the identical droplet resonator while varying ΔP_{in} in a range of 20 ~ 200 μW and for the most strongly coupled resonance in each spectrum, we extracted the corresponding values of ΔP_{in} and $\Delta\lambda_{res}$. Our experiments were conducted using four different laser scanning speeds (V_{scan}) to see if there is any time-dependent response of the WGM-induced nonlinearity and each experimental result (grey dots) is shown in Figs. 3(a)-(d), respectively, where the statistical distribution of each result is represented by black errorbar. The blue dashed curves are simulation results based on the HO model, where we numerically solved the coupled Eqs. (1), (2.1), and (2.2) using the following parameters: $\tau_r = \tau_c = 0.997$ (resulting in $Q = 1.5 \times 10^6$), $\mu = 15$ mPa · s, $\sigma = 18$ mN/m, and $P_{sat} = 2048$ W. Unless specified otherwise, the same parameters were used for all subsequent HO analyses. Though the experimentally observed WGMs exhibited huge variations in their coupling ratios ($\Delta P_{in}/P_{in}$) in under-coupled regime, the simulation considered only the case of critical coupling by setting $\tau_r = \tau_c$ for simplicity, where P_{WGM} is independent of the coupling ratio as long as ΔP_{in} remains constant. The values of these WGM coupling coefficients were correspondingly chosen by Eq. (2.2) to reproduce the average value of the measured Q factor. P_{sat} was determined by applying the steady-state analysis in our previous work [30] with the optofluidic parameters of our droplet resonator. Consequently, among all these HO parameters, only σ and μ remained as

Optics EXPRESS

fitting parameters and their values were chosen to be in a practically similar order of material properties of our droplet fluid.

Both the experimental result and simulation showed that for slower scans (Figs. 3(a)-(c) at $V_{scan} = 1.17$, 2.33, and 3.50 nm/s), the relationship between $\Delta\lambda_{res}$ and ΔP_{in} was mostly linear ($\Delta\lambda_{res}/\Delta P_{in} \sim 60$ pm/mW), which can be justified as follows. For a WGM circulating within the droplet, its power attenuation can be estimated as $\Delta P_{WGM} = \alpha 2\pi R P_{WGM}$ according to [38], and its value must be equal to ΔP_{in} at steady state. The decay constant (α), including all types of optical losses in the resonator, was determined from the attenuation coefficient of WGM (τ_r) as $\alpha = -\ln(\tau_r)/(\pi R) = 3.8\ m^{-1}$, where the τ_r could also be estimated from the experimentally measured Q of resonator as $\tau_r = \sqrt{1 - 2\pi^2 n_{core} R_0/Q\lambda}$. In conjunction with $\Delta\lambda_{res}/\lambda = P_{WGM}/P_{sat}$, we now have a simple linear estimation of resonance shift $\Delta\lambda_{res} \approx \Delta P_{in}\lambda/(\alpha 2\pi R P_{sat})$ and such estimates are shown as dashed red lines in Figs. 3(a)-(d). Unlike the results at slower laser scans, for the fastest scan ($V_{scan} = 7.00$ nm/s) in Fig. 3(d), our result suggested that $\Delta\lambda_{res}$ remained almost unchanged for relatively low ΔP_{in}<100 μW and then rapidly increased once ΔP_{in} exceeded 100 μW. Such threshold-like behavior was originated from our method of transmission spectrum

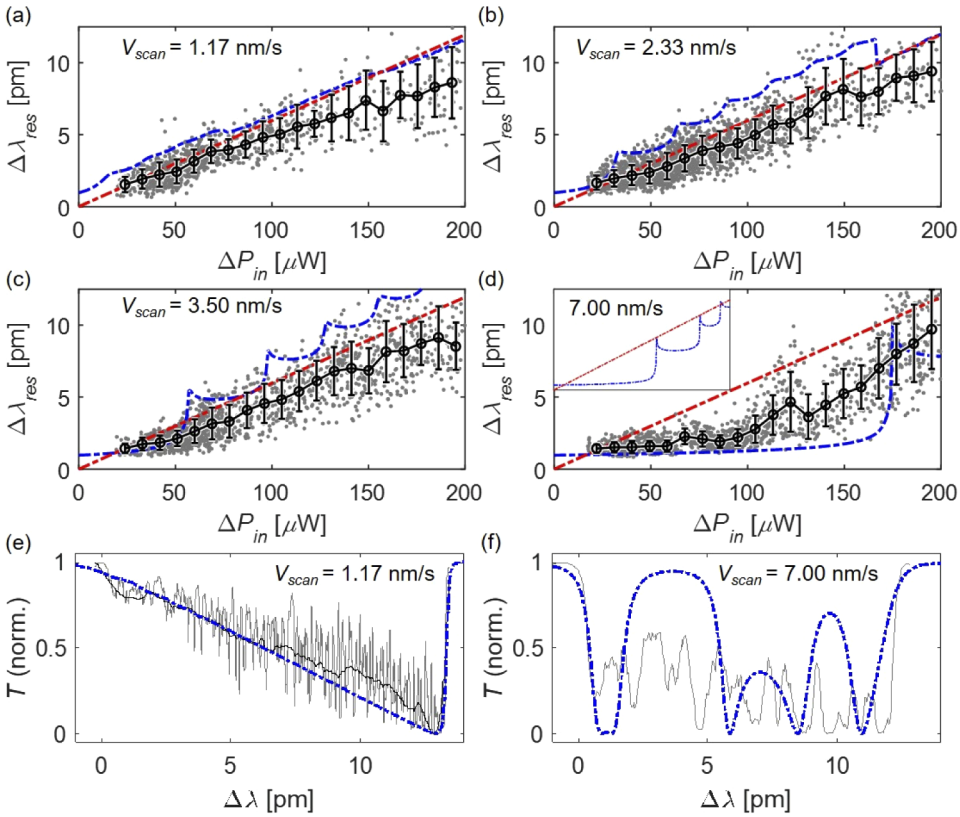

Fig. 3. Experimental result of radiation pressure-induced nonlinearity during up-scan. (a-d) Radiation pressure-induced resonance shift at different input power and laser scan speeds: V_{scan} = (a) 1.17 nm/s, (b) 2.33 nm/s, (c) 3.50 nm/s, (d) 7.00 nm/s (grey dots: experimental result, black errorbars: statistical distribution of grey dots, blue dashed curve: HO model, red dashed line: linear estimation). In (d), simulation results for ΔP_{in} up to 300 μW is added as an inset. (e, f) WGM transmission spectra at different up-scan speeds: V_{scan} = (e) 1.17 nm/s, (f) 7.00 nm/s. (grey solid curve: experimental observation, blue dashed curve: HO model)

Optics EXPRESS

scan in that ΔP_{in} (so as the radiation pressure) should be strong enough for the resonance shift induced by droplet deformation to be able to catch up with the speed of laser scan. For the experimental results in Figs. 3(a)-(d), the R-squared of linear regressions are, respectively, 0.48, 0.59, 0.58, and -0.11, which also draw a clear boundary lying between the trend of resonance shifts in slow and fast scans. The typical Q-factors of resonances analysed in Figs. 3(a)-(d) were approximately in a range of $1 \times 10^6 \sim 2 \times 10^6$ and the deviation was attributed to the impurity in core and cladding liquids as well as different mode orders of coupled WGMs.

The V_{scan} dependence of dynamic resonance shift can also be seen from the shape of measured transmission spectra. Figure 3(e) shows a typical slow-scanned WGM transmission spectrum (grey solid) as well as the corresponding simulation (blue dashed), where we normalized the off- (on-) resonanace transmission to be 1 (0). To facilitate the comparison, the noisy result was low pass filtered to minimize the impact of noises introduced by pump laser and thermal fluctuation, and the resulted spectrum is also shown as black solid curve. For such slow scans, the laser wavelength could match the shift of WGM resonance (due to radiation pressure), and then they could smoothly move in tandem and shift towards longer wavelength. On the other hand, the spectrum in Fig. 3(f) was more typical during the fast scans, which more likely exhibits significant fluctuation in droplet radius as well as the transmission, due to the abrupt increase in radiation pressure by the sudden approach of laser wavelength towards the resonance. Here, the difference in the results of Figs. 3(e) and (f), which was detected in a time scale of a few ms or μs, is not assumed to be originated from the Kerr nonlinearity whose ultrafast response is on the order of sub-nanosecond (GHz or THz regime) [41,42], which therefore, would result in almost the same transmission patterns under the abovediscussed different speeds of laser scans through a resonance, e.g., ~14 μs for 7 nm/s scan through a resonance FWHM of 0.1 pm. The same analogy also applies to the distinct trends of Figs. 3(a) and (d), which should not be different under the consideration of Kerr nonlinearity. In addition, our previous theoretical analyses [30–32] also proved that the Kerr nonlinearity of carbon disulfide (CS_2) droplet, known for its high third order nonlinear susceptibility ($\chi^{(3)} = 3.1 \times 10^{-20} m^2/V^2$), in the same configuration as our liquid droplet resonator, is still at least two orders of magnitude lower than the scale of radiation pressure-induced nonlinearity.

To estimate the magnitude of thermally induced resonance fluctuation observed in Fig. 3(e), the equatorial radius of a spherical droplet was assumed to change from R_0 to $R_0 + \Delta R$. Assuming a spheroid shape for the deformed droplet, the increase in droplet's surface area (ΔS) can be approximated as $\Delta S = \Delta S_{spheroid} - \Delta S_{sphere} \cong 20\Delta \cdot R^2$ (valid for ΔR<10 μm within 2% error), which should increase the surface energy of the droplet by $\sigma \Delta S = 20\sigma \Delta R^2$. Equating this energy change to the thermal energy, we could estimate the scale of thermally induced radius fluctuation as $\Delta R_{therm} \cong \sqrt{k_B T_K / 20\sigma} \cong 1$ by assuming $\sigma = 18\ mN/m$ and $T_K = 300\ K$. For the 250 μm radius droplet, the corresponding thermally induced fluctuation of WGM resonance wavelength ($\Delta\lambda_{therm}$) is approximately ±0.3 pm. This simple calculation provides a correct order-of-magnitude estimate of the noise floor in our $\Delta\lambda_{res}$ measurements in Figs. 3(a)-(d).

4.2. Resonance spectra during down-scan

In contrast to the broadened resonances found in up-scan measurements, we obtained resonances with similar or even narrower FWHMs during down-scans. This is because, while the laser wavelength was decreased during the down scan, the radiation pressure still pushed the droplet outwards and shifted the WGM resonance to the opposite. In an extreme case of high ΔP_{in} and slow V_{scan}, such crossover interaction could leave only a sharp spike in the scanned trasnmission spectrum. Figure 4(a) shows the power dependence of the FWHM of WGM resonance ($\Delta\lambda_{FWHM}$) during the down-scan with four different values of V_{scan} in different colours. Markers and dashed curves represent, respectively, the experimentally measured FWHMs and HO model results. Each experimental data point is an average of 5 to 20 FWHM measurements at the similar

Optics EXPRESS

range of ΔP_{in}. This analysis could be meaningful only in statistical manner due to the resulted ultra-sharp FWHMs, which are nearly comparable to the spectral resolution limit. We could also use the HO model to simulate the similar narrowing of WGM FWHMs during down-scans, where the parameters are set to be the same as those used in up-scan analysis (Fig. 3). In general, the degree of FWHM reduction was related to the speed of droplet deformation and was more pronounced when higher ΔP_{in} (stronger force acting on droplet surface) and slower V_{scan} (longer time for surface acceleration) were used. For faster droplet deformation, the resonance wavelength crossed over the laser wavelength in a shorter time and left a narrower shape of resonance in the transmission spectrum. Similar to the discussion in up-scan analysis, the time scale of resonance shift during down-scan is also found to be comparable with the laser scan (microseconds), exhibiting no correlation with the Kerr nonlinearity.

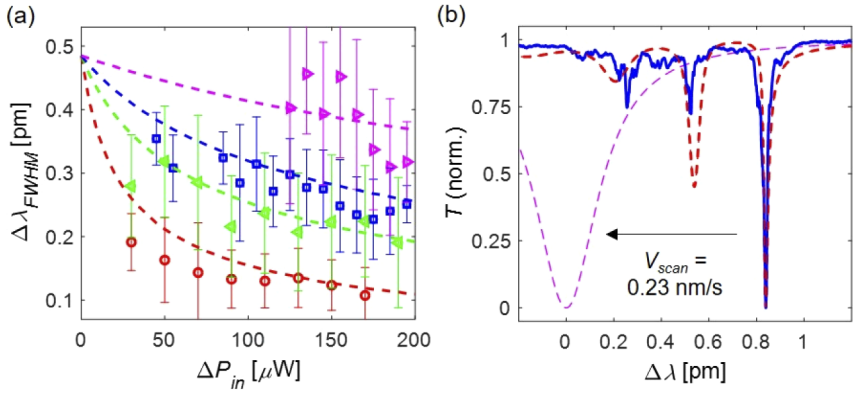

Fig. 4. Spectral pattern of WGM transmission during downscan. (a) FWHM of squeezed resonance during down-scan at scan speeds: V_{scan} = red: 1.17 nm/s, green: 2.33 nm/s, blue: 3.50 nm/s, magenta: 7.00 nm/s. (markers: experimental result, dashed lines: HO model) (b) WGM transmission spectra during down-scan. (blue: experimental result, red: HO model, magenta: cold resonance).

In addition, an interesting "ringing" transmission spectrum was observed during down-scan, as shown in Fig. 4(b) by the blue solid curve (HO model: $\tau_r = \tau_c = 0.998$ (resulting in $Q = 2.3\times10^6$), $\Delta P_{in} = 100$ μW, $V_{scan} = 0.23$ nm/s). The three decaying dips represent the multi-crossing of laser wavelength through a single resonance whose location as well as the radius of droplet are time-varying, where such oscillatory motion is modulated by the coupled optical power of WGM. As the laser wavelength approached from the red-side tail of cold resonance, a fraction of WGM started to be excited, and the resulting radiation pressure shifted the resonance toward a higher wavelength, thereby enforcing even stronger coupling. Even for a short time after the laser wavelength passed the shifted on-resonance (major dip in spectrum), there was an additional increase in resonance wavelength due to the inertial motion of droplet surface. Such a process triggered a "slingshot" motion of droplet surface, where soon the shifted resonance recovered back toward the cold resonance by means of the surface tension of droplet. In contrast to the first encounter, the second encounter (second dip in spectrum) was made by the chase of recovering resonance from the red-side of laser wavelength. The second encounter again red-shifted the resonance and the same process was repeated until the laser wavelength completely passed the original location of resonance.

In conjunction with the fluctuating transmission spectrum in Fig. 3(f), the frequency of such interaction between laser wavelength and resonance is found to be around 1 kHz, which is close to the natural frequency of the previously reported octane drop resonator in water [26], where the study attributed the emergence of oscillation in WGM transmission to the interaction of surface

Optics EXPRESS

tension and centrifugal radiation pressure as well. Therefore, above observation of dynamic oscillatory interplay between the surface energy of droplet and WGM induced radiation pressure was distinguishable from the others seen in relaxation type thermal nonlinearities, i.e., thermal expansion, thermo-optic effect [38,39], and viscous flow induced by light scattering force [43].

5. Discussion

With the optical resonance modes, i.e., WGMs, coupled into the unique design of droplet resonator in all-liquid platform, it was confirmed that, not only an excitation of radiation pressure-induced nonlinearity with a low optical power, but the control of its magnitude and the measurement of following optomechanical responses were also feasible. Moreover, by controlling the time scale and direction of spectral scan through the WGM resonance, we could reach a conclusion that our observation of the interplay between droplet geometry and optical energy by means of radiation pressure is clearly distinguishable from other kinds of nonlinearities. More importantly, the measured scales of resonance shift and droplet deformation at given optical powers closely matched with our theoretical predictions, where we now continue the unique finding with a discussion of single-photon-level nonlinearity.

Based on our previous theoretical predictions and abovementioned analyses, the saturation powers (P_{sat}) for droplets with different radii are estimated as shown in Fig. 5(a), where we considered liquids with normal ($\sigma = 18\ mN/m$) as well as two ultralow but experimentally attainable interfacial tensions ($\sigma = 1$ and 10^{-2} mN/m) by using microemulsion [17]. Figure 5(b) shows the magnitude of droplet deformation ($\Delta R/R_0$) induced by the radiation pressure of a single photon in that we set the total energy within the droplet to be $\hbar\omega$. Two features are immediately obvious from Figs. 5(a) and (b): 1) The strength of nonlinearity is inversely proportional to the σ; and 2) the effective nonlinearity scales as $\sim 1/R_0^2$ and is much stronger for smaller droplets. For instance, in a liquid droplet with $R_0 \sim 30\ \mu$m and $\sigma = 10^{-2}\ m$N/m, the presence of a single photon can generate $\Delta R \sim 39$ nm and $\Delta\lambda_{res} \sim 1$ nm. Given our experimental data in Fig. 3, such a large resonance shift should be clearly measurable. Furthermore, under such conditions, droplet deformation induced by a single photon becomes comparable, yet remains larger than the thermal fluctuation at room temperature $\Delta R_{therm} = \sqrt{k_B T_K/20\sigma} \sim 5$ nm, signifying the single-photon-level nonlinearity at room temperature.

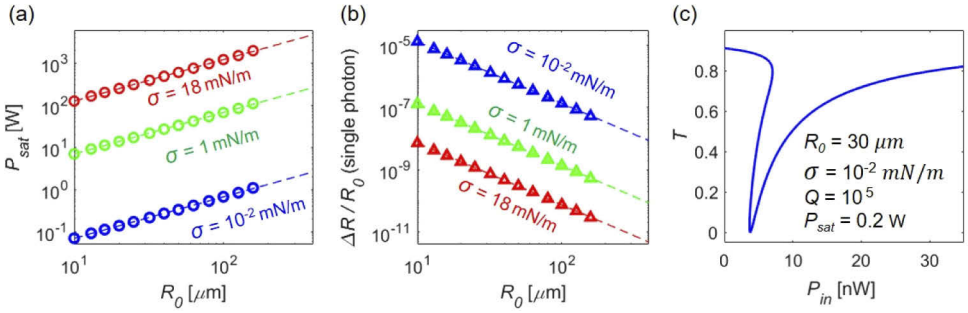

Fig. 5. Theoretical analysis of the feasibility of single-photon nonlinearity. (a) The saturation power P_{sat} for droplets with different radii and surface tensions. (b) The change of droplet radius due to the presence of a single-photon versus droplet radius at different interfacial tensions. (c) Optical bistability for a droplet with low interfacial tension.

It should be noted that our study scales the radiation pressure-induced nonlinearity by the equilibrium change in the radius of droplet, not the instantaneous response, where the cavity ring-down time ($\tau = Q/\omega$) is yet considered. Such a steady-state operation requires continuous injection of optical power into the resonator, and when it comes to our abovementioned condition

Optics EXPRESS

'presence of single photon in a resonator', there needs to be an input power equal to the single photon energy ($\hbar\omega$) divided by its lifetime (τ). For example, the ring-down time of a WGM resonator with $Q = 10^5$ at $\lambda = 780$ nm is 0.41 ns, and the equivalent input power becomes approximately $\hbar\omega/\tau = 0.6$ nW. In that context, we carefully made our choice of the term 'single-photon-*level* nonlinearity' rather than simply 'single-photon nonlinearity' throughout our work.

Last but not least, adopting the novel concept of recently reported Kerr-induced optical bistability [44–48] to our study of radiation pressure-induced nonlinearity, we could also expect all-optical switching in single-photon-level [49–51]. For example, given the value of $P_{sat} = 0.2$ W estimated in Fig. 5(a) at the abovementioned droplet parameters ($R_0 \sim 30$ μm and $\sigma = 10^{-2}$ mN/m), the steady-state transmission of a droplet resonator with $Q = 10^5$ (use of relatively lower level of Q-factor due to the consideration of potential increase in scattering loss induced by ultralow surface tension) can be calculated by combining Eqs. (1), (2.1), and (2.2) as shown in Fig. 5(c). Interestingly, the transmission coefficient becomes multivalued at $P_{in} \sim 5$ nW, which resembles broadly reported characteristic feature of the optical bistability. At this power level, the energy of WGM in the droplet approximately corresponds to the single-photon energy.

Funding

Directorate for Engineering (1438112, 1919753).

Disclosures

The authors declare no conflicts of interest.

References

1. T. J. Kippenberg and K. J. Vahala, "Cavity Optomechanics: Back-Action at the Mesoscale," Science **321**(5893), 1172–1176 (2008).
2. M. Aspelmeyer, T. J. Kippenberg, and F. Marquardt, "Cavity optomechanics," Rev. Mod. Phys. **86**(4), 1391–1452 (2014).
3. A. Cho, "Putting Light's Light Touch to Work As Optics Meets Mechanics," Science **328**(5980), 812–813 (2010).
4. D. Brooks, T. Botter, S. Schreppler, T. P. Purdy, N. Brahms, and D. M. S.-Kurn, "Non-classical light generated by quantum-noise-driven cavity optomechanics," Nature **488**(7412), 476–480 (2012).
5. J. Hofer, A. Schliesser, and T. J. Kippenberg, "Cavity optomechanics with ultrahigh-Q crystalline microresonators," Phys. Rev. A **82**(3), 031804 (2010).
6. S. Tallur, S. Sridaran, and S. A. Bhave, "A monolithic radiation-pressure driven, low phase noise silicon nitride opto-mechanical oscillator," Opt. Express **19**(24), 24522–24529 (2011).
7. G. Anetsberger, O. Arcizet, Q. P. Untterreithmeier, R. Riviere, A. Schliesser, E. M. Weig, J. P. Kotthaus, and T. J. Kippenberg, "Near-field cavity optomechanics with nanomechanical oscillators," Nat. Phys. **5**(12), 909–914 (2009).
8. R. Riviere, S. Deleglise, S. Weis, E. Gavartin, O. Arcizet, A. Schliesser, and T. J. Kippenberg, "Optomechanical sideband cooling of a micromechanical oscillator close to the quantum ground state," Phys. Rev. A **83**(6), 063835 (2011).
9. G. I. Harris, D. L. McAuslan, E. Sheridan, Y. Sachkou, C. Baker, and W. P. Bowen, "Laser cooling and control of excitations in superfluid helium," Nat. Phys. **12**(8), 788–793 (2016).
10. E. Gil-Santos, C. Baker, D. T. Nguyen, W. Hease, C. Gomez, A. Lemaitre, S. Ducci, G. Leo, and I. Favero, "High-frequency nano-optomechanical disk resonators in liquids," Nat. Nanotechnol. **10**(9), 810–816 (2015).
11. G. Bahl, K. H. Kim, W. Lee, J. Liu, X. Fan, and T. Carmon, "Brillouin cavity optomechanics with microfluidic devices," Nat. Commun. **4**(1), 1994 (2013).
12. K. Y. Fong, M. Poot, and H. X. Tang, "Nano-Optomechanical Resonators in Microfluidics," Nano Lett. **15**(9), 6116–6120 (2015).
13. A. Ashkin and J. M. Dziedzic, "Radiation pressure on a free liquid surface," Phys. Rev. Lett. **30**(4), 139–142 (1973).
14. I. I. Komissarovak, G. V. Ostrovskaya, and E. N. Shedova, "Light pressure induced deformations of a free liquid surface," Opt. Commun. **66**(1), 15–20 (1988).
15. A. Casner, J.-P. Delville, and I. Brevik, "Asymmetric optical radiation pressure effects on liquid interfaces under intense illumination," J. Opt. Soc. Am. B **20**(11), 2355–2362 (2003).
16. A. Casner and J.-P. Delville, "Giant Deformations of a Liquid-Liquid Interface Induced by the Optical Radiation Pressure," Phys. Rev. Lett. **87**(5), 054503 (2001).

Optics EXPRESS

17. A. Casner and J.-P. Delville, "Adaptive lensing driven by the radiation pressure of a continuous-wave laser wave upon a near-critical liquid-liquid interface," Opt. Lett. **26**(18), 1418–1420 (2001).
18. J.-Z. Zhang and R. K. Chang, "Shape distortion of a single water droplet by laser-induced electrostriction," Opt. Lett. **13**(10), 916–918 (1988).
19. H. M. Lai, P. T. Leung, K. L. Poon, and K. Young, "Electrostrictive distortion of a micrometer-sized droplet by a laser pulse," J. Opt. Soc. Am. B **6**(12), 2430–2437 (1989).
20. J. M. Hartings, X. Pu, J. L. Cheung, and R. K. Chang, "Laser-induced distortion for increased input coupling of light to droplet-cavity modes," J. Opt. Soc. Am. B **14**(11), 2842–2849 (1997).
21. A. Jonas, Y. Karadog, M. Mestre, and A. Kiraz, "Probing of ultrahigh optical Q-factors of individual liquid microdroplets on superhydrophobic surfaces using tapered optical fiber waveguides," J. Opt. Soc. Am. B **29**(12), 3240–3247 (2012).
22. M. H.-Zadeh and K. J. Vahala, "Fiber-taper coupling to Whispering-Gallery modes of fluidic resonators embedded in a liquid medium," Opt. Express **14**(22), 10800–10810 (2006).
23. S. Kaminski, L. L. Martin, and T. Carmon, "Tweezers controlled resonator," Opt. Express **23**(22), 28914–28919 (2015).
24. S. T. Attar, V. Shuvayev, L. Deych, L. L. Martin, and T. Carmon, "Level-crossing and modal structure in microdroplet resonators," Opt. Express **24**(12), 13134–13141 (2016).
25. S. Maayani, L. L. Martin, and T. Carmon, "Water-walled microfluidics for high-optical finesse cavities," Nat. Commun. **7**(1), 10435 (2016).
26. S. Kaminski, L. L. Martin, S. Maayani, and T. Carmon, "Ripplon laser through stimulated emission mediated by water waves," Nat. Photonics **10**(12), 758–761 (2016).
27. S. Maayani, L. L. Martin, S. Kaminski, and T. Carmon, "Cavity optocapillaries," Optica **3**(5), 552–555 (2016).
28. R. Dahan, L. L. Martin, and T. Carmon, "Droplet optomechanics," Optica **3**(2), 175–178 (2016).
29. A. Giorgini, S. Avino, P. Malara, P. D. Natale, M. Yannai, T. Carmon, and G. Gagliardi, "Stimulated Brillouin Cavity Optomechanics in Liquid Droplets," Phys. Rev. Lett. **120**(7), 073902 (2018).
30. Y. Xu, P. Zhang, S. Jung, and A. Lee, "Analysis of radiation pressure induced nonlinear optofluidics," Opt. Express **22**(23), 28875–28889 (2014).
31. P. Zhang, S. Jung, A. Lee, and Y. Xu, "Comparative analysis of nonlinear optofluidic processes in microdroplets," Phys. Rev. E **93**(6), 063119 (2016).
32. P. Zhang, S. Jung, A. Lee, and Y. Xu, "Radiation-pressure-induced nonlinearity in microdroplets," Phys. Rev. E **92**(6), 063033 (2015).
33. I. Brevik and R. Kluge, "Oscillations of a water droplet illuminated by a linearly polarized laser pulse," J. Opt. Soc. Am. B **16**(6), 976–985 (1999).
34. S. Ellingsen, "Theory of microdroplet and microbubble deformation by Gaussian laser beam," J. Opt. Soc. Am. B **30**(6), 1694–1710 (2013).
35. B. E. Little, J.-P. Laine, and H. A. Haus, "Analytic Theory of Coupling from Tapered Fibers and Half-Blocks into Microsphere Resonators," J. Lightwave Technol. **17**(4), 704–715 (1999).
36. K. Qian, J. Tang, H. Guo, W. Liu, J. Liu, C. Xue, Y. Zheng, and C. Zhang, "Under-coupling Whispering Gallery Mode Resonator Applied to Resonant Micro-Optic Gyroscope," Sensors **17**(12), 100 (2017).
37. H. M. Lai, P. T. Leung, and K. Young, "Limitations on the photon storage lifetime in electromagnetic resonances of highly transparent microdroplets,"," Phys. Rev. A **41**(9), 5199–5204 (1990).
38. I. Teraoka, "Analyssi of thermal stabilization of whispering gallery mode resonance," Opt. Commun. **310**, 212–216 (2014).
39. T. Carmon, L. Yang, and K. J. Vahala, "Dynamical thermal behavior and thermal self-stability of microcavities," Opt. Express **12**(20), 4742–4750 (2004).
40. A. Yariv, "Universal relations for coupling of optical power between microresonators and dielectric waveguides," Electron. Lett. **36**(4), 321–322 (2000).
41. D. Mcmorrow, W. Lotshaw, and G. K.-Wallace, "Femtosecond Optical Kerr Studies on the Origin of the Nonlinear Responses in Simple Liquids," IEEE J. Quantum Electron. **24**(2), 443–454 (1988).
42. J. Pfeifle, V. Brasch, M. Lauermann, Y. Yu, D. Wegner, T. Herr, K. Hartinger, P. Schindler, J. Li, D. Hillerkuss, R. Schmogrow, C. Weimann, R. Holzwarth, W. Freude, J. Leuthold, T. J. Kippenberg, and C. Koos, "Coherent terabit communications with microresonator Kerr frequency combs," Nat. Photonics **8**(5), 375–380 (2014).
43. D. Bar-david, S. Maayani, L. Martin, and T. Carmon, "Cavity optofluidics: a µdroplet's whispering-gallery mode makes a µvortex," Opt. Express **26**(15), 19115–19122 (2018).
44. H. Guo, M. Karpov, E. Lucas, A. Kordts, M. H. P. Pfeiffer, V. Brasch, G. Lihachev, V. E. Lobanov, M. L. Gorodetsky, and T. J. Kippenberg, "Universal dynamics and deterministic switching of dissipative Kerr solitons in optical microresonators," Nat. Phys. **13**(1), 94–103 (2017).
45. V. B. Braginsky, M. L. Gorodetsky, and V. S. Inchenko, "Quality-factor and nonlinear properties of optical whispering-gallery modes," Phys. Lett. A **137**(7-8), 393–397 (1989).
46. M. M. Mazumder, S. C. Hill, D. Q. Chowdhury, and R. K. Chang, "Dispersive optical bistability in a dielectric sphere," J. Opt. Soc. Am. B **12**(2), 297–310 (1995).

Optics EXPRESS

47. D. L. Creedon, M. E. Tobar, J.-M. L. Floch, Y. Reshtnyk, and T. Duty, "Single-crystal sapphire resonator at millikelvin temperatures: Observation of thermal bistability in high-Q factor whispering gallery modes," Phys. Rev. B **82**(10), 104305 (2010).
48. F. R.-Manzano, N. Prtljaga, L. Pavesi, G. Pucker, and M. Ghulinyan, "Thermo-optical bistability with Si nanocrystals in a whispering gallery mode resonator," Opt. Lett. **38**(18), 3562–3565 (2013).
49. P. Lodahl, S. Mahmoodian, S. Stobbe, A. Rauschenbeutel, P. Schneeweiss, J. Volz, H. Pichler, and P. Zoller, "Chiral quantum optics," Nature **541**(7638), 473–480 (2017).
50. S. Sun, H. Kim, Z. Luo, G. Solomon, and E. Waks, "A single-photon switch and transistor enabled by a solid-state quantum memory," Science **361**(6397), 57–60 (2018).
51. T. Volz, A. Reinhard, M. Winger, A. Badolato, K. J. Hennessy, E. L. Hu, and A. Imamoglu, "Ultrafast all-optical switching by single photons," Nat. Photonics **6**(9), 605–609 (2012).